

000  
001  
002  
003  
004  
005  
006  
007054  
055  
056  
057  
058  
059  
060  
061  
062  
063  
064  
065  
066  
067  
068  
069  
070  
071  
072  
073  
074  
075  
076  
077  
078  
079  
080  
081  
082  
083  
084  
085  
086  
087  
088  
089  
090  
091  
092  
093  
094  
095  
096  
097  
098  
099  
100  
101  
102  
103  
104  
105  
106  
107

# Lung Disease Classification - Applied AI Final Report

Group-Q

## Abstract

Chest X-rays scans are among the most accessible ways to diagnose lung diseases. This study tries to compare the detection of lung diseases using these scans from three different datasets using deep neural networks. Three different backbone architectures, ResNet34, MobileNet V3 Large and EfficientNet B1 were used along with a set of models trained using transfer learning. It is observed that MobileNet takes the least amount of time to train while ResNet converges the fastest. Also, EfficientNet performs the best most of the times on Chest X-ray scans. An F1 score of 0.8 for the pneumonia dataset was obtained, 0.98 for the COVID-19 dataset and 0.46 for the multilabel chest X-ray 8 dataset. Finally, models are visualized using t-SNE and gradCAM to understand the features learned by the models and correlate them with the actual effect of the diseases on the lungs.

## 1. Introduction

Early diagnosis of respiratory diseases like pneumonia and COVID-19 leads to decreased mortality rate [8] and is a powerful way to manage a pandemic [46]. These diseases can be diagnosed using a variety of tests like pulse oximetry, chest x-ray, CT scan [38], PCR [2] however chest X-rays are by far the most accessible [12] to low and middle income countries. Furthermore, the scan is available in minutes making it one of the fastest ways of diagnosis [39]. However, the bottleneck with this method is the need for an expert radiologists to evaluate the scan [30]. Many researchers have tried to solve this problem by creating a deep learning based lung disease classification system [43] but haven't been able to come up with models that can replace radiologists. Small [15] and highly imbalanced data [43], along with varying specifications of X-ray scanners leading to low inter-hospital accuracy [36] are the biggest problems that researchers have faced. Another issue with using deep neural networks in medical settings is its black-box nature, doctors and patients will not trust a model that cannot explain its results [31].

This project is an attempt to compare three CNN backbone architectures namely, ResNet-34, MobileNet V3 Large and EfficientNet B1 along with three lung disease datasets to identify the type of architecture that

works best for lung disease classification. Two of the datasets used presented a multiclass classification problem with 3 classes while the third dataset presented a multiclass, multilabel classification problem. A total of 12 models were trained in this study, four for each of the three datasets. The first three models for each dataset was trained from scratch and the fourth model was trained using transfer learning. Transfer learning was performed by deep-tuning ImageNet weights and the performance was evaluated to check improvement over the models trained from scratch. The small dataset problem and the issue of different radiographic contrast [32] is mitigated using data augmentation. Imbalanced data problem is handled by undersampling the majority class. The hyperparameters were fixed across models and the F1 scores, cross entropy loss was used to compare models and select the best overall model. All the models were optimized using the Adam optimizer [23] with default parameters. The cosine annealing [29] learning rate scheduler was used to decrease the learning rate as training progressed. Further, an ablation study was performed to find the best learning rate for the selected model. Finally, Grad-CAM [14] and T-SNE were used to visualize the trained models and understand model predictions better. This would help shed light on the black box nature of the models and allow subject matter experts to trust the predictions better. An F1 score of 0.8 and 0.98 was achieved for the two multiclass datasets, whereas the maximum F1 for the multilabel dataset with 7 classes was 0.46.

**Related Works:** Li *et al.* [26] were among the first to use CNNs in a medical setting. They used a single convolutional layer to classify interstitial lung diseases using CT scans, achieving better performance than existing state of the art approaches. Since then there has been a dramatic increase in application of CNNs in the healthcare setting, deep neural networks have been used to perform various tasks like segmenting regions of interest in MRI scans [9, 21], classifying X-Ray [35], MRI [11], and CT [3] scans. Further, GANs have been used to generate high quality scans [28] when there is a lack of available data due to either privacy reasons or unavailability of subjects. GANs have also been used to generate high quality CT scans from MRI scans [27]. Apart from radiographic scans, deep CNNs have also been used to detect malarial parasite in blood smear

108	Dataset	No. of Images	Classes	Size
109	COVID [6, 7, 34]	3.6k:3.6k:1.3k	3	299 <sup>2</sup>
110	Pneumonia [22, 41]	3k:1.5k:1.5k	3	224 <sup>2</sup>
111	Chest X-Ray8 [44, 45]	7.2k:7k:7k:4.1k :3.9k:3.5k:2.9k	7	1024 <sup>2</sup>

Table 1. Shortlisted Datasets.

images [42] with an accuracy of 99.96%. Another interesting application is the use of 1-D convolutions to detect heart anomalies using ECG data [24] collected using smartwatches. These models can be trained once for a patient and can be used to give radiologist level prediction on the go. Researchers have also used architectures like the Inception V3 to perform dermatologist level skin-cancer detection using skin lesion images [10] using transfer learning.

In the recent years, many researchers have tried to predict lung diseases using deep CNNs, Wang *et al.* [44] used state of the art backbone architectures to train a lung disease classifier for multilabel data by training only the prediction and transition layers from scratch and leaving pre-trained ImageNet weights freezed while training. They achieved a high AUC of over 0.6 for most of the classes in the dataset with this technique. Rajpurkar *et al.* [35] created a 121 layer deep CNN - CheXNet to detect pneumonia using chest X-rays with radiologist level accuracy. Labhane *et al.* [25] used transfer learning with state of the art backbone architectures like VGG16, VGG19 and InceptionV3 to predict pneumonia in pediatric patients and achieved an F1 score of 0.97. Islam *et al.* combined CNN and LSTM to create a COVID-19 detector [19]. The CNN extracted complex features from scans and the LSTM was used as a classifier. This method resulted in an improvement over a vanilla CNN network and an F1 score of 98.9% was achieved. Abbas *et al.* [1] created the DeTraC network to detect COVID in chest X-rays that improved performance of existing backbone models significantly with the highest accuracy of 98.23% using the VGG19 architecture. Guefrechi *et al.* [15] on the other hand used data augmentation techniques like random rotation, flipping and noise with transfer learning on backbone architectures like ResNet50, InceptionV3 and VGG16 to achieve a high accuracy of 98.3%.

In the following sections methodology of the approach and the results will be discussed.

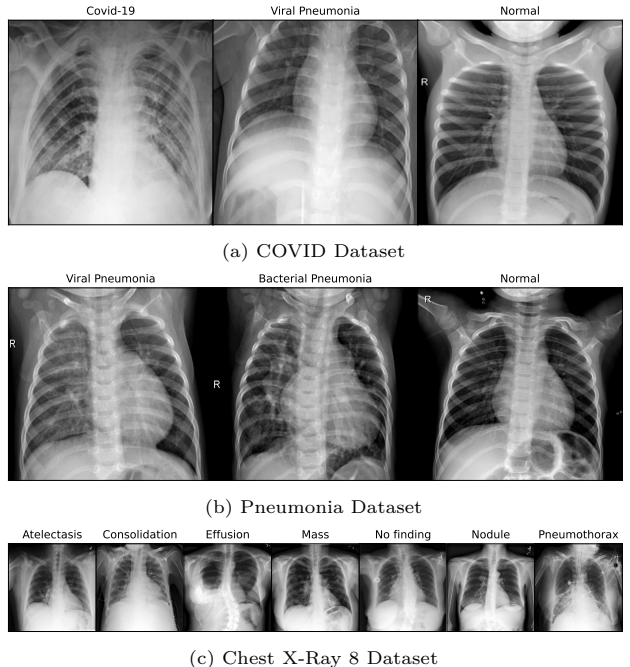


Figure 1. Sample Chest X-rays from the datasets used.

## 2. Methodology

**Datasets:** (Tab. 1) with varying disease types were chosen to ensure model robustness and to get results across a set of different diseases. Other criteria included the *number of images per class* and *image quality* as noisy scans can lead to mis-diagnosis [37].

The **COVID** dataset was created by a team of researchers from Qatar University, Doha, Qatar, and the University of Dhaka, Bangladesh along with collaborators from Pakistan and Malaysia in collaboration with medical doctors from the Italian Society of Medical and Interventional Radiology database using 43 different publications [6, 7, 34]. It is a multiclass data with three classes, COVID, viral pneumonia and normal. X-rays with widespread, hazy, and irregular ground glass opacities are of the COVID-19 class [20]. Whereas, the ones with haziness only in the lower regions [47] are viral pneumonia cases as shown in Fig. 1. Chest X-rays of normal lungs provide a clear view of the lungs. The normal class was undersampled to use only 3.6k scans and reduce the data imbalance.

The **Pneumonia**, dataset contains scans from pediatric patients of one to five year olds collected as part of patients' routine clinical care at the Guangzhou Women and Children's Medical Center, Guangzhou, China. [22, 41] This dataset is multiclass with three classes, viral pneumonia, bacterial pneumonia and normal. Scans with one white condensed area affect-



Figure 2. Effect of pre-processing on Chest X-ray images.

ing only one side of the lungs are tagged as bacterial pneumonia [4] as bacteria tends to aggressively attack one part of the lungs causing inflammation to replace the cells that were otherwise filled with air. On the other hand, X-rays which show bilateral patchy areas of consolidation are classified as viral pneumonia [16] as viruses attack both sides of the lungs producing a homogeneous inflammatory reaction causing mucus and cellular debris. Normal scans here as well produce a clear view of the lungs.

NIH released over 100k anonymized chest X-ray images along with their radiological reports from over 30k patients. Wang *et al.* [44] used this data to create the **Chest X-ray 8** dataset by generating disease labels through NLP from the radiological reports. [45] The dataset contains 15 classes but only 7 (Fig. 1) were chosen for this study. This dataset is significantly different from the other two as it is a multilabel dataset, thus the same image can be labelled as two different classes. Classes were iteratively removed, ensuring that they are not highly imbalanced to finally reach the 7 classes. With over 29,000 images of size 1024 x 1024, this dataset was the biggest and thus had to be resized down to 384 x 384 to reduce training and processing times. Furthermore, normal class images were undersampled by first choosing one scan per patient and then selecting 7,000 scans out of this subset randomly. The data consists of multiple scans from the same subject which could lead to data leakage between the train, val and test sets if a random train-test-val split was performed. This was prevented with the use of Group-ShuffleSplit from the scikit library to keep scans from the same patient in the same split.

Before training, all the images were pre-processed using histogram equalization and Gaussian blur with a 5x5 filter as Gielczyk *et al.* [13] showed that this improved the F1 score by about 4% for the chest X-ray classification task. Visually, the contrast of the scan improved and allowed irregularities to stand out as shown in Fig. 2. Next, the scans were divided into train, validation and test with the 70:15:15 split. During training, the scans were augmented using Ran-

Arch.	Params (Mil.)	Layers	FLOPS (Bil.)	Imagenet Acc.	
MobileNet	5.5	18	8.7	92.6	270 271 272 273 274 275 276 277
EfficientNet	7.8	25	25.8	94.9	278 279 280 281 282 283 284 285 286 287
Resnet	21.8	34	153.9	91.4	288 289 290 291 292 293 294 295 296 297 298 299 300 301 302 303 304 305 306 307 308 309 310 311 312 313 314 315 316 317 318 319 320 321 322 323

Table 2. Shortlisted Backbone Architectures.

domAdjustSharpness and RandomAutocontrast in Pytorch to increase the number of images the model gets to learn from and ensure that the model is robust to scans from different machines. RandomHorizontalFlip was also used to make the models invariant to the direction of the scan as some scans were anterior-posterior while others were posterior-anterior [5].

**Backbone Architectures:** (Tab. 2) of various configuration and blocks were chosen to ensure that different ideas are tested in this study. Other selection criteria were the *number of trainable parameters*, important to keep track of the total training time, *FLOPS* as models that could easily be deployed on to embedded devices were required and the *top 5 classification accuracy* on the ImageNet 1K benchmark dataset.

**ResNet 34** residual learning network with 34 layers that are made possible by skip connections. The 34 layer variant was chosen to decrease training time while not compromising on the accuracy much. This architecture had the highest trainable parameters and FLOPS while the lowest Imagenet accuracy. [17]

**MobileNet V3 Large** uses depthwise separable convolution from MobileNet V2 along with squeeze-excitation blocks in residual layers from MnasNet. This makes it really quick to train while still performing at par with other architectures. This architecture had the lowest trainable parameters and FLOPS among the three selected. Howard *et al.* [18] also used network architecture search to find the most effective model. The large configuration was chosen to not compromise on the prediction accuracy.

**EfficientNet B1** uses compound scaling to scale the model by depth, width and resolution. The B1 version was chosen to have faster training without compromising on the accuracy. [40] This architecture performs the best among the selected on the Imagenet benchmark dataset while having a third of the trainable parameters of Resnet34.

**Optimization Algorithm:** The Adam optimizer [23] is an adaptive learning rate algorithm which was chosen as the algorithm of choice as it converges faster by integrating benefits of RMSProp and momentum. It is also robust to hyperparameters but, requires tweak-

ing of the learning rate depending on the task at hand. For this study, a learning rate of 0.01 and the author recommend settings for  $\beta_1 = 0.9$ ,  $\beta_2 = 0.999$  and  $\epsilon = 10^{-8}$  were used for the first and second order moment estimate as defined in Eq. (1) and Eq. (2) where  $\beta_1$  and  $\beta_2$  control the decay rates.

$$m_t = \beta_1 \cdot m_{t-1} + (1 - \beta_1) \cdot g_t \quad (1)$$

$$v_t = \beta_2 \cdot v_{t-1} + (1 - \beta_2) \cdot g_t^2 \quad (2)$$

Further, the Cosine annealing [29] learning rate scheduler was used to reduce the learning rate as the training progressed down to a low of 0.001.

### 3. Results

#### Experiment Setup:

First undersampling was performed as described in Sec. 2 on the datasets. Then, the scans were pre-processed using histogram equalization and Gaussian blur before resizing them and storing them in separate directories to make it easier for PyTorch dataloaders. Two datasets in this study presented the multiclass classification problem while the third, chest X-ray 8 dataset presented the multiclass, multilabel classification problem. Thus, the training methodology was separated for these two problems. For the multilabel problem, a softmax layer had to be added before the loss function to get 0 or 1 prediction for all the classes of the data. For this, the BCEWITHLOGITSLOSS function of PyTorch was used as it combines the Sigmoid layer and the BCELoss function in one single class. This makes theses operations more numerically stable than their separate counterparts [33]. The backbone architectures were obtained directly from the torchvision library and the final classification layer was modified for the selected datasets. For the models which had to be trained from scratch, the weights were randomly initialized and the entire model was trained for a total of 100 epochs each. For the transfer learning models, the weights were initialized with the IMAGENET1K\_V2 weights but the entire model was fine-tuned. The rationale behind performing deep-tuning was that the Imagenet data is very different from chest X-ray scans thus the model would need to learn features from X-ray scans.

The batch size was fixed to 32 for all the models. While training, the best model by validation loss was saved to prevent the usage of overfit models for test set analysis. The actual and predicted results from each epoch was also stored to calculate the F1 score at each step of training. While calculating the F1 score, macro averaging was used to get an average score

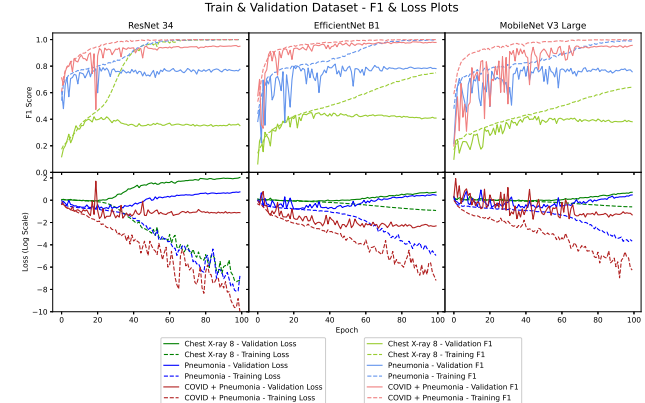


Figure 3. Train & Val, F1 & Loss plots for the 9 models.

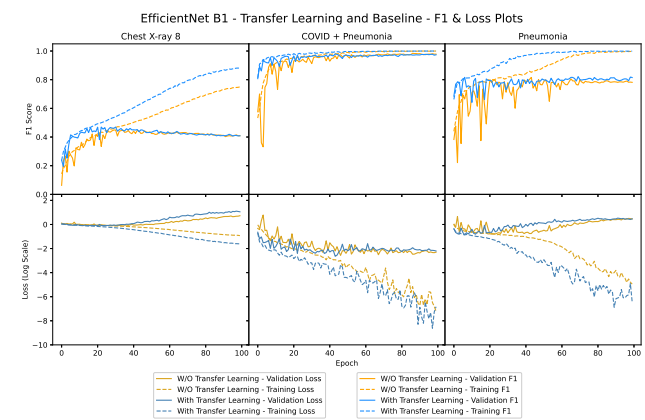


Figure 4. Train & Val, F1 & Loss plots for EfficientNet trained from scratch and with ImageNet weights.

across classes. All images were normalized before getting trained with the mean and standard deviation of the training set of each of the selected datasets.

Initial training runs of the multilabel data produced a zero F1 score due to its highly imbalanced nature. To mitigate this, class wise weights were calculated and used with the loss function. This improved the F1 score considerably.

Finally, the best models from each run by validation loss were used to get the test set metrics that are displayed in Tab. 3. Training and validation F1 score and loss are also provided in Fig. 3 and Fig. 4.

#### Main Results:

From Fig. 3 it is clear that going from a smaller architecture to a bigger architecture, makes the model start to overfit earlier. The MobileNet model was the most unstable among the three and also took more epochs to reach the minima. The EfficientNet algorithm performs best for the COVID and Chest X-ray 8 dataset and all three architectures performed simi-

Model	ResNet			MobileNet			EfficientNet			EN - Transfer Learning		
Dataset	F1	Time	Epoch	F1	Time	Epoch	F1	Time	Epoch	F1	Time	Epoch
Pneumonia	0.784	82	<b>22</b>	<b>0.804</b>	<b>75</b>	42	0.768	110	44	0.782	114	70
COVID	0.959	50	<b>21</b>	0.967	<b>37</b>	44	<b>0.979</b>	56	46	0.978	56	43
X-Ray 8	0.411	11,502	<b>19</b>	0.406	<b>7,275</b>	42	0.445	13,820	31	<b>0.457</b>	13,813	29

Table 3. F1 (higher is better), time per epoch in seconds (lower is better), and number of epochs to reach the best validation loss (lower is better) for the 12 models that were trained.

lar for the pneumonia dataset. This shows that the compound scaling of EfficientNet gives good results for chest X-ray data. The X-ray 8 dataset performed the worst among the three datasets which could be due to the high number of classes, class imbalance and the multilabel nature of the problem. Surprisingly, the pneumonia dataset performed worse than the COVID + pneumonia dataset which indicates that COVID cases are easier to distinguish from pneumonia cases.

In Fig. 4 it can be seen that the transfer learning model had a much better start than the randomly initialized model. It also converged much quicker than the model trained from scratch. For the Pneumonia dataset, the model trained from scratch was highly unstable at the start and could not catch up to the transfer learning model even after 100 epochs in terms of the F1 score.

Finally, looking at Tab. 3 it can be seen that the MobileNet architecture was the fastest to train per epoch. It consistently took less time per epoch but, if number of epochs required to converge is considered, it does not train the fastest all the time. It is also evident that ResNet converged the fastest at half the number of epochs compared with other models. EfficientNet models perform the best in terms of the overall F1 score on the test set with the exception of the Pneumonia dataset where surprisingly MobileNet performed the best. The transfer learning models converged quicker than the other models with the exception of the Pneumonia dataset. Another surprising observation is that the EfficientNet model takes the longest to train per epoch even though the number of trainable parameters is nowhere close to ResNet. Also, MobileNet isn't as fast to train as expected when compared to ResNet even though it has 4 times the learnable parameters. This could be due to two reasons, depthwise convolutions are not optimized in the version of PyTorch and CUDA used and training is getting CPU bound due to the data augmentation before each training run which would take the same amount of time for all the models.

Fig. 5 shows that the models are able to differentiate well between the normal and pneumonia classes but struggle with the viral pneumonia vs bacterial pneu-

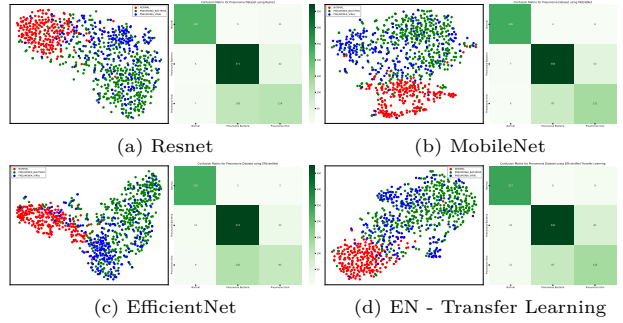


Figure 5. T-SNE and Confusion matrices for the test set of the Pneumonia dataset.

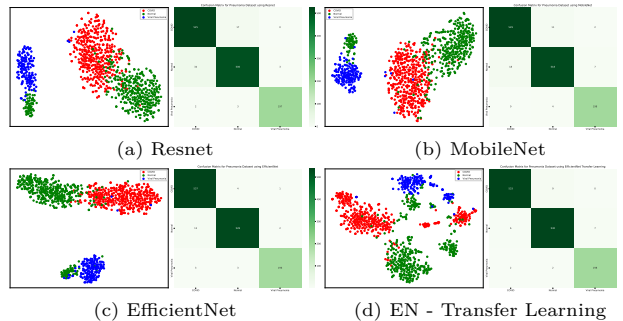
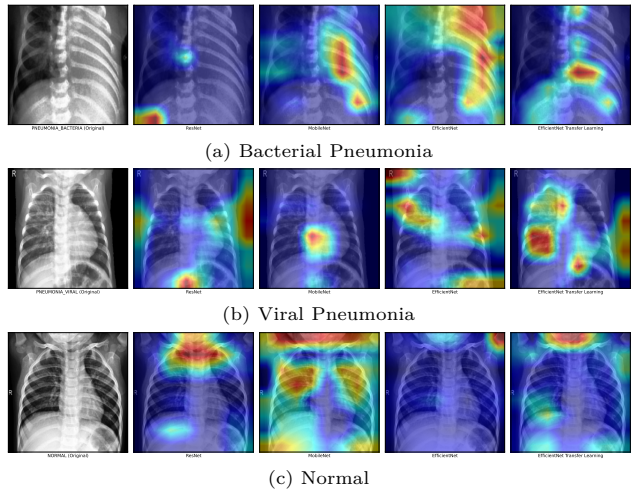


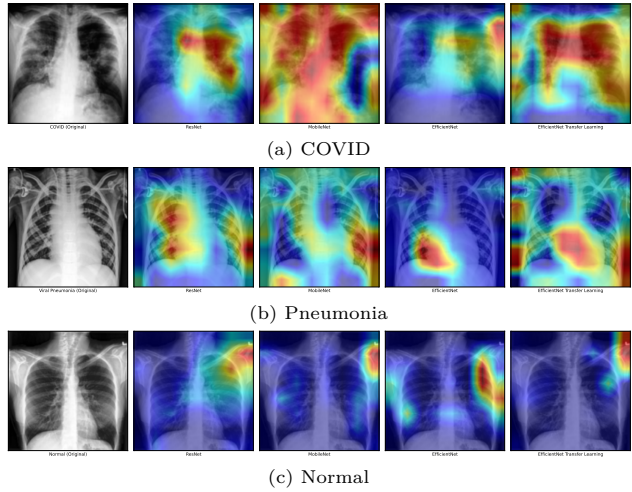
Figure 6. T-SNE and Confusion matrices for the test set of the COVID dataset.

monia classification. MobileNet performs better but the EfficientNet transfer learning model creates better separation of classes. Thus, even though MobileNet performs better in this case, the EfficientNet transfer learning model would generalize well on new unseen data. This is correlated in the confusion matrix where the transfer learning and MobileNet models perform the best.

Fig. 6 shows that all models do a good job of separating classes to create distinct clusters but, the transfer learning model creates better clusters with separate smaller clusters. These smaller clusters could indicate other factors of the disease, for example the severity and amount of lung damage caused by the disease. This performance of the transfer learning model can be confirmed by looking at the confusion matrix as well.



556 Figure 7. GradCAM visualization for the Pneumonia  
557 dataset.  
558



576 Figure 8. GradCAM visualization for the COVID dataset.  
577  
578

579 Fig. 7 shows the gradCAM visualization of the last  
580 layer of the convolutional network. Here it can be seen  
581 that ResNet is learning completely different features  
582 as compared to the other models. This could be the  
583 reason for its low performance. In case of bacterial  
584 pneumonia, the network identifies affected area on the  
585 right side of the scan. On the other hand, in case of vi-  
586 ral pneumonia, models look at both sides of the lungs.  
587 This correlates with the actual progression of these  
588 diseases as given in Sec. 2.

589 Fig. 8 shows that MobileNet activates the entire im-  
590 age incase of COVID, this could be the reason for its  
591 low performance. In case of pneumonia, the Efficient-  
592 Net models identifies affected areas on the bottom of  
593 the lungs. On the other hand, in case of COVID, the

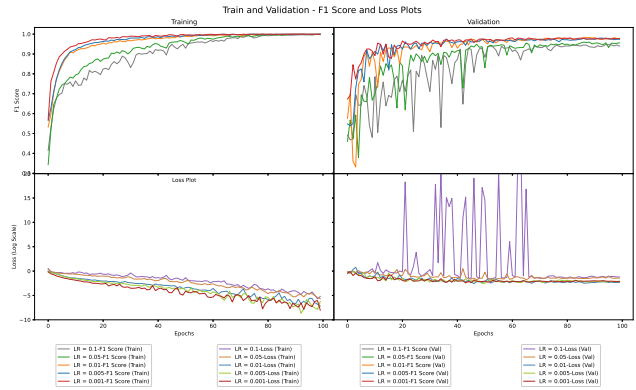


Figure 9. Train & Val, F1 & Loss plots for ablative study models.

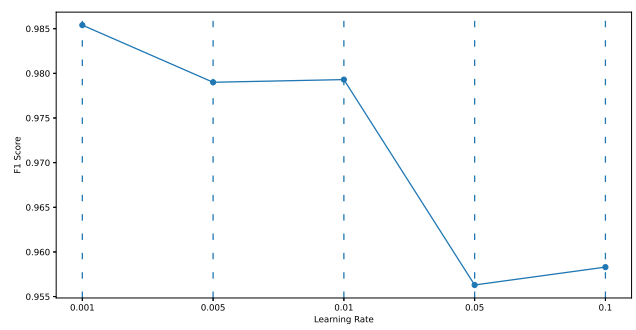


Figure 10. Ablative Study F1 scores (Higher is better).

models look at a bigger region of the lungs. This correlates with how these diseases impact the lungs as given in Sec. 2.

**Ablative Study:** For the ablative study, the COVID dataset was chosen along with the EfficientNet B1 architecture trained from scratch. The learning rates chosen for the study are 0.001, 0.005, 0.01, 0.05, and 0.1. From the training and validation F1 score and loss plots given in Fig. 9 it is seen that a very high learning rate of 0.1 is highly unstable and prevents the model from reaching close to global minima. Similarly, learning rate of 0.05 also prevented the model from converging on the validation set even after 100 epochs. The other three learning rates all converged on the validation set but, the learning rate of 0.001 was the most stable and reached the highest F1 score earliest. On the other hand, learning rate of 0.01 performed marginally better on the loss plot. From Fig. 10 it can be seen that the best performing learning rate is 0.001 on the F1 score of the test set with 0.005, 0.01 close seconds and 0.05, 0.1 performing the worst. This matches the results of the validation set on Fig. 9. Thus, a learning rate of 0.001 performs the best on the COVID dataset with transfer learning.

648

649  

## References

650

651

652

653

654

655

656

657

658

659

660

661

662

663

664

665

666

667

668

669

670

671

672

673

674

675

676

677

678

679

680

681

682

683

684

685

686

687

688

689

690

691

692

693

694

695

696

697

698

699

700

701

- [1] Asmaa Abbas, Mohammed M Abdelsamea, and Mohamed Medhat Gaber. Classification of covid-19 in chest x-ray images using detrac deep convolutional neural network. *Applied Intelligence*, 51(2):854–864, 2021. 2
- [2] Noorullah Akhtar, Jiyuan Ni, Claire Langston, Gail J Demmler, and Jeffrey A Towbin. Pcr diagnosis of viral pneumonitis from fixed-lung tissue in children. *Biochemical and molecular medicine*, 58(1):66–76, 1996. 1
- [3] Wafaa Alakwaa, Mohammad Nassef, and Amr Badr. Lung cancer detection and classification with 3d convolutional neural network (3d-cnn). *International Journal of Advanced Computer Science and Applications*, 8(8), 2017. 1
- [4] How Drugs are Made and Product List. Viral vs. bacterial pneumonia: Understanding the difference. [https://www.pfizer.com/news/articles/viral\\_vs\\_bacterial\\_pneumonia\\_understanding\\_the\\_difference](https://www.pfizer.com/news/articles/viral_vs_bacterial_pneumonia_understanding_the_difference), 2020. 3
- [5] Aleksander Botev, Matthias Bauer, and Soham De. Regularising for invariance to data augmentation improves supervised learning. *arXiv preprint arXiv:2203.03304*, 2022. 3
- [6] Muhammad E. H. Chowdhury, Tawsifur Rahman, Amith Khandakar, Rashid Mazhar, Muhammad Abdul Kadir, Zaid Bin Mahbub, Khandakar Reajul Islam, Muhammad Salman Khan, Atif Iqbal, Nasser Al Emadi, Mamun Bin Ibne Reaz, and Mohammad Tariqul Islam. Can ai help in screening viral and covid-19 pneumonia? *IEEE Access*, 8:132665–132676, 2020. 2
- [7] Muhammad E. H. Chowdhury, Tawsifur Rahman, Amith Khandakar, Rashid Mazhar, Muhammad Abdul Kadir, Zaid Bin Mahbub, Khandakar Reajul Islam, Muhammad Salman Khan, Atif Iqbal, Nasser Al Emadi, Mamun Bin Ibne Reaz, and Mohammad Tariqul Islam. Covid-19 radiography database. <https://www.kaggle.com/datasets/tawsifurrahman/covid19-radiography-database>, 2021. 2
- [8] Priya Daniel, Chamira Rodrigo, Tricia M Mckeever, Mark Woodhead, Sally Welham, and Wei Shen Lim. Time to first antibiotic and mortality in adults hospitalised with community-acquired pneumonia: a matched-propensity analysis. *Thorax*, 71(6):568–570, 2016. 1
- [9] Jose Dolz, Karthik Gopinath, Jing Yuan, Herve Lombaert, Christian Desrosiers, and Ismail Ben Ayed. Hyperdense-net: a hyper-densely connected cnn for multi-modal image segmentation. *IEEE transactions on medical imaging*, 38(5):1116–1126, 2018. 1
- [10] Andre Esteva, Brett Kuprel, Roberto A Novoa, Justin Ko, Susan M Swetter, Helen M Blau, and Sebastian Thrun. Dermatologist-level classification of skin cancer

- with deep neural networks. *nature*, 542(7639):115–118, 2017. 2
- [11] Ammarah Farooq, SyedMuhammad Anwar, Muhammad Awais, and Saad Rehman. A deep cnn based multi-class classification of alzheimer’s disease using mri. In *2017 IEEE International Conference on Imaging systems and techniques (IST)*, pages 1–6. IEEE, 2017. 1
- [12] Guy Frija, Ivana Blažić, Donald P Frush, Monika Hierath, Michael Kawooya, Lluis Donoso-Bach, and Boris Brkljačić. How to improve access to medical imaging in low-and middle-income countries? *EClinicalMedicine*, 38:101034, 2021. 1
- [13] Agata Gielczyk, Anna Marciniak, Martyna Tarczewska, and Zbigniew Lutowski. Pre-processing methods in chest x-ray image classification. *Plos one*, 17(4):e0265949, 2022. 3
- [14] Jacob Gildenblat and contributors. Pytorch library for cam methods. <https://github.com/jacobgil/pytorch-cam>, 2021. 1
- [15] Sarra Guefrechi, Marwa Ben Jabra, Adel Ammar, Anis Koubaa, and Habib Hamam. Deep learning based detection of covid-19 from chest x-ray images. *Multimedia Tools and Applications*, 80(21):31803–31820, 2021. 1, 2
- [16] W Guo, J Wang, M Sheng, M Zhou, and L Fang. Radiological findings in 210 paediatric patients with viral pneumonia: a retrospective case study. *The British journal of radiology*, 85(1018):1385–1389, 2012. 3
- [17] Kaiming He, Xiangyu Zhang, Shaoqing Ren, and Jian Sun. Deep residual learning for image recognition. In *Proceedings of the IEEE conference on computer vision and pattern recognition*, pages 770–778, 2016. 3
- [18] Andrew Howard, Mark Sandler, Grace Chu, Liang-Chieh Chen, Bo Chen, Mingxing Tan, Weijun Wang, Yukun Zhu, Ruoming Pang, Vijay Vasudevan, et al. Searching for mobilenetv3. In *Proceedings of the IEEE/CVF international conference on computer vision*, pages 1314–1324, 2019. 3
- [19] Md Zabirul Islam, Md Milon Islam, and Amanullah Asraf. A combined deep cnn-lstm network for the detection of novel coronavirus (covid-19) using x-ray images. *Informatics in medicine unlocked*, 20:100412, 2020. 2
- [20] Adam Jacobi, Michael Chung, Adam Bernheim, and Corey Eber. Portable chest x-ray in coronavirus disease-19 (covid-19): A pictorial review. *Clinical imaging*, 64:35–42, 2020. 2
- [21] Baris Kayalibay, Grady Jensen, and Patrick van der Smagt. Cnn-based segmentation of medical imaging data. *arXiv preprint arXiv:1701.03056*, 2017. 1
- [22] Daniel Kermany, Kang Zhang, Michael Goldbaum, et al. Labeled optical coherence tomography (oct) and chest x-ray images for classification. *Mendeley data*, 2(2), 2018. 2
- [23] Diederik P Kingma and Jimmy Ba. Adam: A method for stochastic optimization. *arXiv preprint arXiv:1412.6980*, 2014. 1, 3

- 756 [24] Serkan Kiranyaz, Turker Ince, and Moncef Gabbouj.  
757 Real-time patient-specific ecg classification by 1-d  
758 convolutional neural networks. *IEEE Transactions on*  
759 *Biomedical Engineering*, 63(3):664–675, 2015. 2
- 760 [25] Gaurav Labhane, Rutuja Pansare, Saumil Maheshwari,  
761 Ritu Tiwari, and Anupam Shukla. Detection of  
762 pediatric pneumonia from chest x-ray images using cnn  
763 and transfer learning. In *2020 3rd International Conference on Emerging Technologies in Computer Engineering: Machine Learning and Internet of Things (ICETCE)*, pages 85–92. IEEE, 2020. 2
- 764 [26] Qing Li, Weidong Cai, Xiaogang Wang, Yun Zhou,  
765 David Dagan Feng, and Mei Chen. Medical image classifi-  
766 cation with convolutional neural network. In *2014 13th international conference on control automation robotics & vision (ICARCV)*, pages 844–848. IEEE, 2014. 1
- 767 [27] Yanxia Liu, Anni Chen, Hongyu Shi, Sijuan Huang,  
768 Wanjia Zheng, Zhiqiang Liu, Qin Zhang, and Xin  
769 Yang. Ct synthesis from mri using multi-cycle gan for  
770 head-and-neck radiation therapy. *Computerized Medical Imaging and Graphics*, 91:101953, 2021. 1
- 771 [28] Mohamed Loey, Florentin Smarandache, and Nour El-  
772 deen M. Khalifa. Within the lack of chest covid-19 x-  
773 ray dataset: a novel detection model based on gan and  
774 deep transfer learning. *Symmetry*, 12(4):651, 2020. 1
- 775 [29] Ilya Loshchilov and Frank Hutter. Sgdr: Stochastic  
776 gradient descent with warm restarts. *arXiv preprint arXiv:1608.03983*, 2016. 1, 4
- 777 [30] P Mehrotra, V Bosemani, and J Cox. Do radiologists  
778 still need to report chest x rays? *Postgraduate medical journal*, 85(1005):339–341, 2009. 1
- 779 [31] Aleksandra Mojsilovic. Introducing ai explainability  
780 360. <https://www.ibm.com/blogs/research/2019/08/ai-explainability-360/>, 2019. 1
- 781 [32] Andrew Murphy. Radiographic contrast. <https://radiopaedia.org/articles/radiographic-contrast>, 2022. 1
- 782 [33] PyTorch. Bce with logits loss. <https://pytorch.org/docs/stable/generated/torch.nn.BCEWithLogitsLoss.html>, 2022. 4
- 783 [34] Tawsifur Rahman, Amith Khandakar, Yazan Qiblawey,  
784 Anas Tahir, Serkan Kiranyaz, Saad Bin Abul Kashem,  
785 Mohammad Tariqul Islam, Somaya Al Maadeed, Susu M.  
786 Zughaier, Muhammad Salman Khan, and Muhammad E.H.  
787 Chowdhury. Exploring the effect of image enhancement  
788 techniques on covid-19 detection using chest x-ray images.  
789 *Computers in Biology and Medicine*, 132:104319, 2021. 2
- 790 [35] Pranav Rajpurkar, Jeremy Irvin, Kaylie Zhu, Brandon  
791 Yang, Hershel Mehta, Tony Duan, Daisy Ding,  
792 Aarti Bagul, Curtis Langlotz, Katie Shpanskaya, et al.  
793 Chexnet: Radiologist-level pneumonia detection on  
794 chest x-rays with deep learning. *arXiv preprint arXiv:1711.05225*, 2017. 1, 2
- 795 [36] Melissa Rohman. Ai performs poorly when  
796 tested on data from multiple health systems.  
797  
798  
799  
800  
801  
802  
803  
804  
805  
806  
807  
808  
809
- 810 <https://healthimaging.com/topics/artificial-intelligence / ai - poorly - detects - pneumonia - chest-x-rays>, 2018. 1
- 811 [37] Janaki Sivakumar, K Thangavel, and P Saravanan.  
812 Computed radiography skull image enhancement us-  
813 ing wiener filter. In *International Conference on Pat-  
814 tern Recognition, Informatics and Medical Engineering  
815 (PRIME-2012)*, pages 307–311. IEEE, 2012. 2
- 816 [38] Matt Smith. Common lung diagnostic tests. <https://www.webmd.com/lung/breathing-diagnostic-tests>,  
817 2022. 1
- 818 [39] Healthwise Staff. Chest x-ray. <https://www.healthlinkbc.ca/tests-treatments-medications/medical-tests/chest-x-ray>, 2021. 1
- 819 [40] Mingxing Tan and Quoc Le. Efficientnet: Rethinking  
820 model scaling for convolutional neural networks. In  
821 *International conference on machine learning*, pages  
822 6105–6114. PMLR, 2019. 3
- 823 [41] Tolga. Chest x-ray images. <https://www.kaggle.com/datasets/tolgadincer/labeled-chest-x-ray-images>, 2020. 2
- 824 [42] Muhammad Umer, Saima Sadiq, Muhammad Ahmad,  
825 Saleem Ullah, Gyu Sang Choi, and Arif Mehmood.  
826 A novel stacked cnn for malarial parasite detection in  
827 thin blood smear images. *IEEE Access*, 8:93782–93792,  
828 2020. 2
- 829 [43] Guangyu Wang, Xiaohong Liu, Jun Shen, Chengdi  
830 Wang, Zhihuan Li, Linsen Ye, Xingwang Wu, Ting  
831 Chen, Kai Wang, Xuan Zhang, et al. A deep-learning  
832 pipeline for the diagnosis and discrimination of viral,  
833 non-viral and covid-19 pneumonia from chest x-ray  
834 images. *Nature biomedical engineering*, 5(6):509–521,  
835 2021. 1
- 836 [44] Xiaosong Wang, Yifan Peng, Le Lu, Zhiyong Lu,  
837 Mohammadkhadi Bagheri, and Ronald M Summers.  
838 Chestx-ray8: Hospital-scale chest x-ray database and  
839 benchmarks on weakly-supervised classification and lo-  
840 calization of common thorax diseases. In *Proceedings  
841 of the IEEE conference on computer vision and pattern  
842 recognition*, pages 2097–2106, 2017. 2, 3
- 843 [45] Xiaosong Wang, Yifan Peng, Le Lu, Zhiyong Lu, Mo-  
844 hammakhadi Bagheri, and Ronald M Summers. Nih  
845 chest x-rays. <https://www.kaggle.com/datasets/nih-chest-xrays/data>, 2017. 2, 3
- 846 [46] Lizhou Xu, Danyang Li, Sami Ramadan, Yanbin Li,  
847 and Norbert Klein. Facile biosensors for rapid de-  
848 tection of covid-19. *Biosensors and Bioelectronics*,  
849 170:112673, 2020. 1
- 850 [47] Na Zhan, Yingyun Guo, Shan Tian, Binglu Huang, Xi-  
851 aoli Tian, Jinjing Zou, Qiutang Xiong, Dongling Tang,  
852 Liang Zhang, and Weiguo Dong. Clinical charac-  
853 teristics of covid-19 complicated with pleural effusion.  
854 *BMC Infectious Diseases*, 21(1):1–10, 2021. 2
- 855  
856  
857  
858  
859  
860  
861  
862  
863